Fabrication and Characteristics of Self-Aligned ZnO Nanotube and Nanorod Arrays on Si Substrates by Atomic Layer Deposition

Yung-Huang Chang, Shun-Min Wang, Chien-Min Liu, and Chih Chen[z]

Department of Materials Science and Engineering, National Chiao-Tung University, Hsinchu 30010, Taiwan

Vertically self-aligned ZnO nanorods and nanotubes are fabricated on Si substrates by atomic layer deposition with the assistance of anodic aluminum oxide at 250°C. These nanostructures are equal in height, isolated, and vertical to the Si substrate. With 550 deposition cycles, we can fabricate regular arrays of ZnO nanorods with an average diameter of 70 nm and with a height of 470 nm. In particular, the wall thickness of the nanotubes can be controlled precisely by using the atomic layer deposition approach. The measured wall thickness is 18.5 ± 1 nm after 250 deposition cycles, which yields a growth rate of 0.075 nm/cycle. A polycrystalline structure for both ZnO nanorods and nanotubes was confirmed by a transmission electron microscope and selected area diffraction pattern. Compared with the ZnO films and nanorods, the fabricated ZnO nanotubes exhibit an excellent performance on photoluminescence characteristics due to their larger surface area.
© 2010 The Electrochemical Society.   [DOI: 10.1149/1.3489953] All rights reserved.

Due to the unique physical and chemical properties, one-dimensional (1D) semiconductor nanostructures have attracted considerable interests in recent years.[1-10] Among them, with various growth methods, a high melting point of 1975°C, thermal and chemical stability at high temperatures, and a wide and direct band-gap semiconductor possessing high excited binding energy of 60 meV, 1D ZnO nanostructures have become one of the most potential materials for optoelectronic devices. Therefore, ZnO can be developed as field emitters,[11] field effect transistors,[12] dye-sensitized solar cells,[13] photodetectors,[14] gas sensors,[15-17] and other optoelectronic devices.[18-21]

In literatures, various techniques have been reported to produce ordered ZnO nanorod or nanotube arrays on substrates, such as metallorganic chemical vapor deposition,[14,19] IR irradiation,[22] thermal evaporation through vapor–liquid–solid[2,3,20,23,24] and vapor–solid mechanisms,[25] electrochemical deposition,[26] hydrothermal chemical method,[27] and template technology.[28,29] Although various growth methods were provided to fabricate nanorod or nanotube arrays, vertically arrayed and wall-thickness controllable 1D ZnO nanostructure on Si substrate is rarely reported. In template-grown technology, anodic aluminum oxide (AAO) has been widely used as a template to prepare 1D self-aligned nanostructure because of a simple fabrication process, low cost, and a high aspect ratio in nanoscale. Furthermore, atomic layer deposition (ALD) is a promising technique possessing a superb capability in precisely controlling the film thickness and in filling pores with high aspect ratios, excellent uniformity, and ~100% step coverage. Therefore, 1D Ru, Al_2O_3, ZnO, and TiO_2 nanostructures can also be prepared by utilizing ALD technology and AAO templates.[30-34] ALD technology has been employed to prepare ZnO nanorod and nanotube arrays.[35,36]

In this paper, we report on a fabrication technique of ZnO nanorod and nanotube arrays using ALD at 250°C and AAO nanoporous templates. Highly ordered ZnO nanorod arrays can be obtained. In particular, self-aligned ZnO nanotube arrays can be fabricated, and their wall thickness is ~18 nm. Their photoluminescence (PL) characteristics were investigated. This approach provides low temperature growth for ZnO nanorod and nanotube arrays with equal height, both vertical to the substrate.

Experimental

To fabricate AAO on a Si substrate, a 20 nm Ti film was deposited on p-type (100) silicon substrates by a sputtering system as adhesion layer. Subsequently, a 1.5 μm thick Al film was deposited by a thermal evaporation coater. A two-step anodization process was fulfilled on the Al film to form a highly ordered nanoporous structure.[37,38] The first anodization was carried out in a 0.3 M oxalic acid ($H_2C_2O_4$) electrolyte at 40 V bias under room temperature. After the first anodization, the AAO film was removed by wet chemical etching at 60°C in a mixed solution of 6 wt % phosphoric acid (H_3PO_4) and 1.8 wt % chromic acid ($H_2Cr_2O_4$) for 40 min. An ordered hexagonal pattern of hemispherical nanoindents was produced on the surface of the aluminum film. The second anodization was performed under the same anodization condition as the first step. Then the AAO layer on the Si substrate was annealed at 400°C for 2 h to improve its quality. A pore widening procedure was accomplished in a 6 wt % H_3PO_4 solution for 30 min. The schematic structure for the sample is shown in Fig. 1a. The as-prepared AAO possessed an average diameter of ~70 nm, a pore distance of ~95 nm, and a height of ~720 nm, and the nanopores have an aspect ratio of 10:2.

Then ALD technique was employed to deposit ZnO into the AAO nanopores. Diethylzinc [DEZ, $Zn(C_2H_5)_2$] and deionized water were used as the precursors for ZnO deposition. Pure N_2 gas (99.999%) was used to carry and purge gas. The reaction is

$$Zn(C_2H_5)_2 + H_2O \rightarrow ZnO + 2C_2H_6 \qquad [1]$$

The reaction chamber was pumped down to 1–2 Torr before deposition. The operating environment of ZnO deposition was maintained at 5 Torr and 250°C. Each deposition cycle consisted of four steps, which included DEZ reactant, N_2 purge, H_2O reactant, and N_2 purge. The typical pulse time for introducing DEZ and H_2O precursors was 1 s, and the N_2 purge time was 1.5 s. The deposition cycles of 180, 250, and 550 cycles were chosen to produce various ZnO nanostructures. The deposition rate at the above condition approaches 0.075 nm/cycle. To fill an AAO pore with 75 nm diameter, at least 500 cycles were needed. Therefore, deposition cycles of 550 was chosen for the growth of ZnO nanorods. We chose 250 and 180 cycles for the fabrication of ZnO nanotubes. A shorter deposition cycle gives a thinner tube wall. After deposition, ZnO film was deposited on the surface of AAO nanopores, as shown in Fig. 1b schematically. With mechanical or sputtering polishing, the ZnO film on the top surface of the AAO can be removed, as shown in Fig. 1c schematically. Finally, the AAO template was selectively removed by a 0.4 wt % sodium hydroxide [NaOH(aq)] solution, and the ZnO nanorod or nanotube arrays can be fabricated on the Si substrate, as shown in Fig. 1d. This approach can produce self-aligned, equal-height, and almost equal-spaced ZnO nanorods and nanotubes on a Si substrate.

The nanostructures of the ZnO arrays were examined by a field-emission-scanning electron microscope (JSM-6500F) and a transmission electron microscope (TEM, JEM-2100F). The PL of the
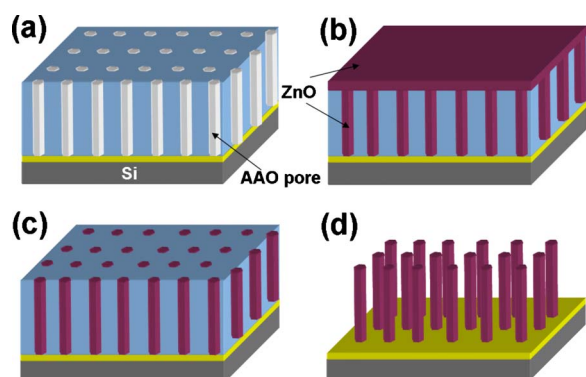
z E-mail: chih@mail.nctu.edu.tw

Figure 1. (Color online) Schematic diagram of the fabrication process for ZnO nanorods and nanotubes: (a) AAO template on a Si substrate, (b) after the deposition of ZnO by ALD, (c) after the procedure of mechanical polishing or sputtering, and (d) after the removal of the AAO template by selective chemical etching.

ZnO nanostructures was measured at room temperature using a continuous wave He–Cd laser of 325 nm wavelength as the excitation source.

Results and Discussion

Figure 2a shows the plan-view scanning electron microscopy (SEM) image of the fabricated AAO. The diameters of the AAO pores range from 65 to 75 nm. Figure 2b shows the cross-sectional
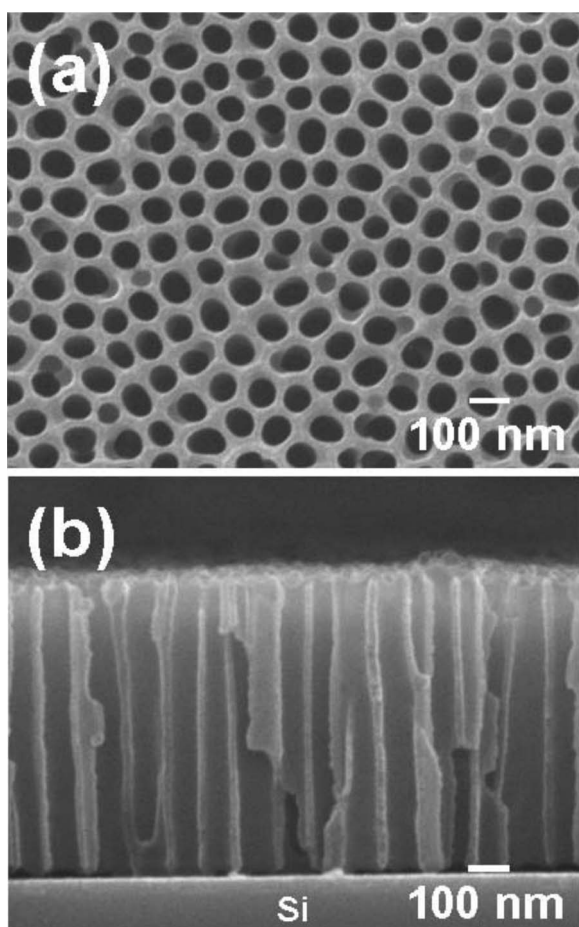

Figure 2. SEM images of the fabricated AAO template: (a) Plan-view, and (b) cross-sectional view.
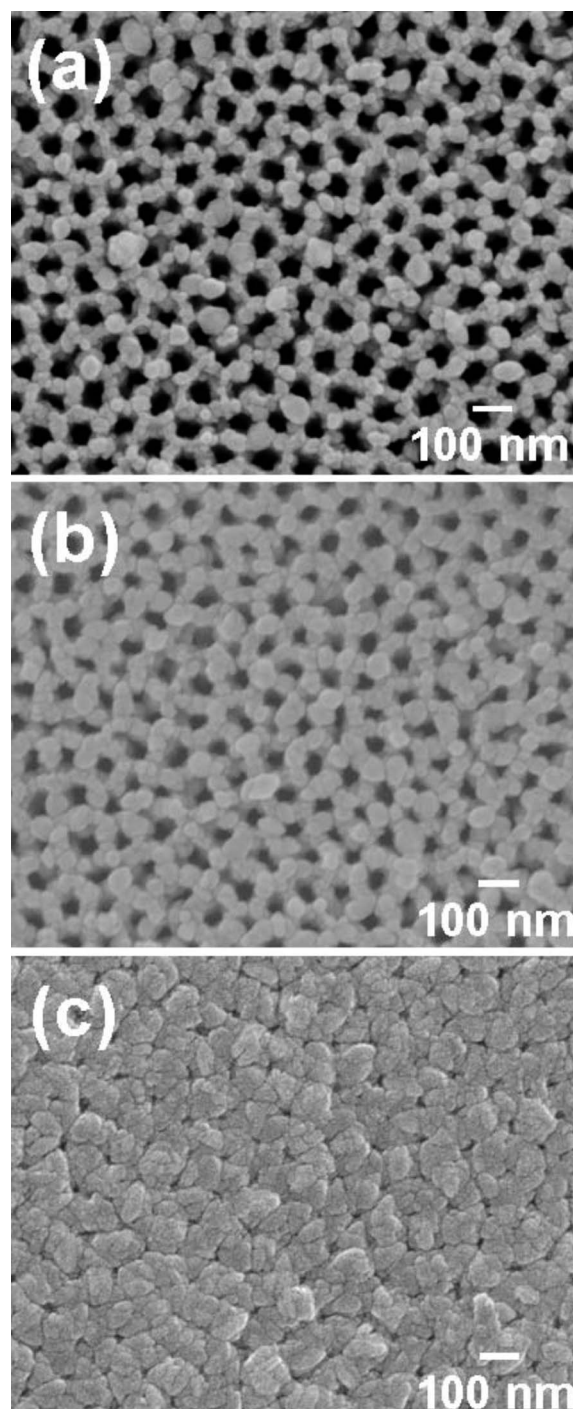

Figure 3. Plan-view SEM images after the ZnO deposition on AAO template for (a) 180, (b) 250, and (c) 550 cycles.

SEM image of the AAO template on a Si substrate. Almost all the pores align vertically to the Si substrate. In particular, the AAO barrier has been removed after the pore widening treatment so that the deposited ZnO nanostructure can stick to the substrate after the removal of the AAO template.

Figure 3a-c shows the plan-view SEM images after the ALD for 180, 250, and 550 cycles, respectively. At 180 cycles, the nanopore structure of the AAO pores could still be clearly observed. Because this growing process belongs to surface reaction control mechanism during the ALD process, the ZnO film can be deposited on the walls, the bottoms, and the top surface of the AAO template uniformly.
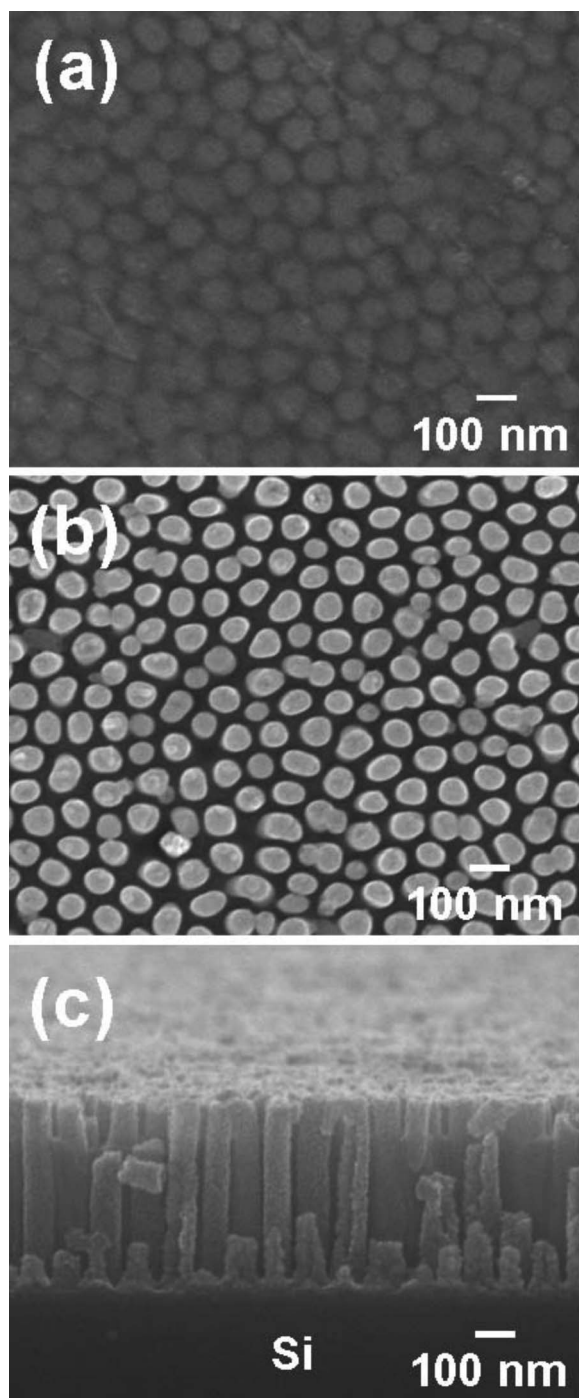
Figure 4. (a) Plan-view SEM image showing the surface morphology of the ZnO nanorods with 550 cycles after mechanical polishing, (b) plan-view SEM image after removing the AAO template, and (c) cross-sectional view of the equal-height ZnO nanorods standing vertically to the Si substrate.

Figure 5. (a) Plan-view SEM images showing the surface morphology of ZnO nanotubes with 250 cycles after mechanical polishing. The open ends of the ZnO nanotubes are filled with the polishing residues. (b) After the selective etching of the AAO template, some of the ZnO nanotubes become visible.

When the deposition cycle increases, the diameters of the AAO pores decrease, as illustrated in Fig. 3b. The AAO pores can be filled completely after 550 cycles, as depicted in Fig. 3c. The AAO pores are no longer visible from the plan-view image after the deposition with 550 cycles.

With mechanical polishing and selective etching, freestanding ZnO nanorods can be fabricated using the sample with 550 cycles. Figure 4a shows the plan-view SEM image after the mechanical polishing on the top surface of the 550 cycle sample in which the lighter area represents the ZnO nanorods and the darker area illus-
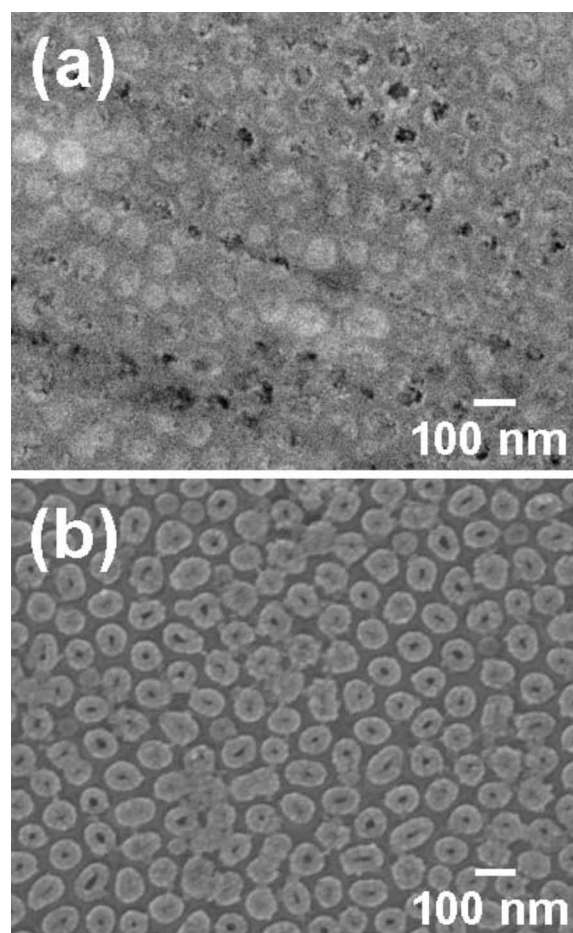
trates the AAO template. After the selective etching of the AAO template by a 0.4 wt % sodium hydroxide [NaOH(aq)] solution, the details of the ZnO nanorods becomes very clear, which is shown in Fig. 4b. All of the nanorods are able to stand firmly and are isolated from each other. To observe their cross-sectional structure, the specimen was cleft and then analyzed by SEM, as shown in Fig. 4c. Because of the cleavage process, some nanorods near the interface were damaged. However, it is quite unique that all the nanorods stand vertically to the Si substrate, and they have the same height of $\sim$470 nm and a uniform diameter of 70 nm.

To fabricate ZnO nanotubes, sputtering etching is required before the selective etching. Otherwise, the open ends of the nanotubes would not be revealed. Figure 5a shows the plan-view SEM image for the 250 cycle sample after the mechanical polishing. Compared with Fig. 3b, the open ends of the nanotubes were blocked by some polishing residues. Thus, no pores were visible after the polishing procedure. With the selective etching, some of the pores may be visible because the etchant also etched away some of the polishing residues, as seen in Fig. 5b. However, compared with Fig. 3b, clearly most of the open ends of the nanotubes were still blocked by the polishing residues. To overcome this difficulty, sputtering etching is employed to etch away the top surface instead of using mechanical polishing. Figure 6a depicts the plan-view SEM image after the sputtering etching by using Ar gas at 150 W for 3 min. Most of the pores of the nanotubes at the upper surface can be observed clearly after the sputtering etching. Figure 6b shows the plan-view
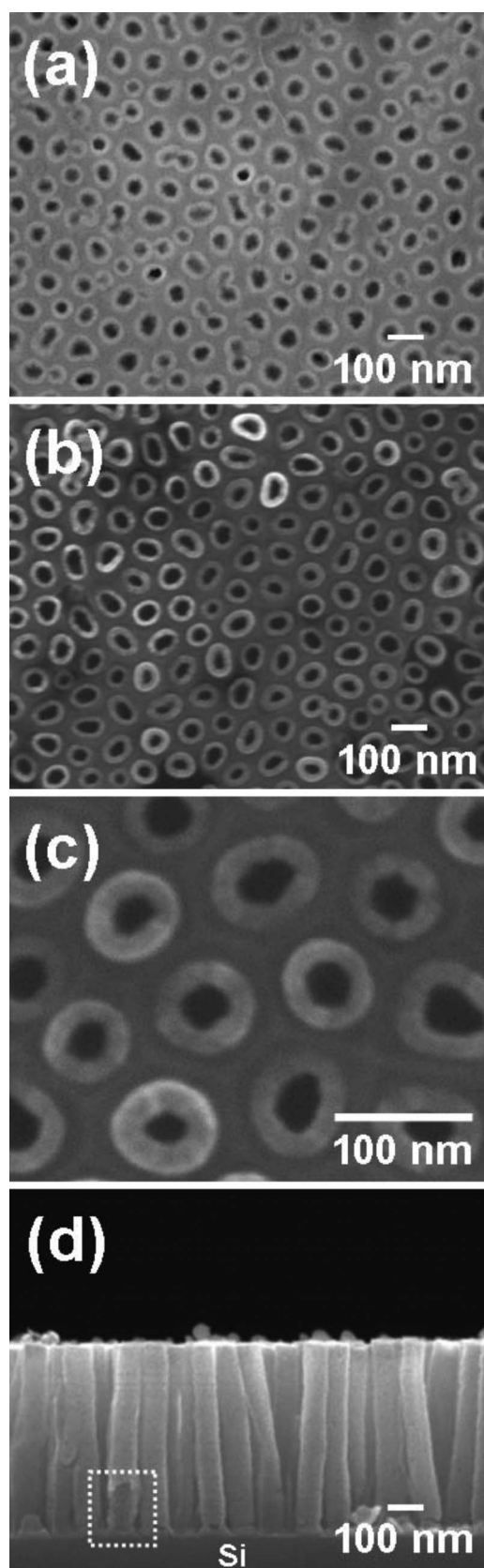
Figure 6. (a) Plan-view SEM image for the ZnO nanotube arrays with 250 cycles after the sputtering etching. (b) After the selective etching of the AAO template for the sample in (a). All the open ends of the nanotubes are revealed using this approach. (c) Enlarged SEM images for the nanotubes in (b). (d) Cross-sectional SEM image after the removal of the AAO template. The dotted square in (d) shows the tube structure clearly.

morphology of the nanotubes after the selective etching of the AAO template. The AAO template did not etch away completely. Almost equal-spaced ZnO nanotubes can be fabricated by using this approach. The thickness of the tube wall appears quite uniform. Figure 6c shows an enlarged image of the nanotubes. The measured wall thickness is 18.5 ± 1 nm under this condition, which yields a growth rate of 0.075 nm/cycle. It is quite unique that the wall thickness is very uniform regardless of the shape of the AAO pores (circles or ovals). Therefore, this approach is quite suitable to fabricate ZnO nanotubes with well-controlled wall thickness.

The ZnO nanotubes can stand firmly even after the complete removal of the AAO template. Figure 6d illustrates the cross-sectional SEM image of the nanotubes. Similar to the ZnO nanorods in Fig. 4c, the nanotubes are of equal height and are almost vertical to the Si substrate. The aspect ratio of the nanotubes reaches 7:4. In particular, the bottoms of the nanotubes remain tubular in structure, as shown in the dotted square in Fig. 6d. The measured thickness of the tube at the bottom is ~ 18.4 nm, which is very close to the mean value of 18.5 ± 1 nm measured from the top of the nanotubes. For the 180 cycle sample, some of the nanotubes were destroyed after the removal of the AAO template. The mechanical strength of the ZnO nanotubes is not strong when the tube wall is too thin; therefore, they may be destroyed during the removal process of the AAO template.

The nanostructures of the nanorods and nanotubes are further investigated by TEM. Figure 7a and b illustrates the cross-sectional TEM images for the ZnO nanotubes (250 cycles) and nanorods (550 cycles) in the AAO template, respectively. For the ZnO nanotubes in Fig. 7a, the tube structure can be observed very clearly in the TEM image and the wall thickness is measured to be ~ 17.4 nm, which corresponds to the measured results from the SEM images. The wall thickness near the top surface is slightly higher than that of the Si substrate. Furthermore, the ALD is capable of filling the AAO pores fully to form ZnO nanorods, as shown in Fig. 7b. The diameter of the nanorods is ~ 70 nm, consistent with the observation from the SEM images. However, some of the nanorods may have tiny voids or seams near the bottom of the nanorods. Yet, in general, the pores were nicely filled, and thus, the ZnO nanorods can be fabricated by using this approach. The ZnO nanorods and nanotubes are polycrystalline. The image contrast in the TEM images represents the different grain orientations. The selected area diffraction patterns are examined in the dotted circles, as shown in Fig. 7c and d. By indexing the diffraction patterns, both the nanorods and nanotubes are identified to be ZnO wurtzite structure. For the ZnO nanotubes, ring patterns with scattered diffraction spots are observed, which are generated from the (100), (101), (102), (110), (103), and (201) planes, as shown in Fig. 7c. The diffraction pattern in Fig. 7d shows clear ring patterns with more diffraction patterns. This may be attributed to the fact that ZnO nanorods comprise more grains than nanotubes in a fixed volume. The polycrystalline characteristics in the ZnO nanostructures are revealed by the ring patterns.

This approach provides an excellent way to fabricate ZnO nanotubes. No other approaches have been reported to fabricate ZnO nanotubes with well-controlled wall thickness, as mentioned in the Introduction. However, when the tube wall is too thin, nanotubes may not be able to stand firmly on the Si substrate. Some possible approaches may be adopted to solve this problem. First, a thinner AAO template could be used. Thus, the aspect ratio of the AAO pores is smaller. The nanotubes may have more chances to remain on the Si substrate after the removal of AAO. The other approach is by not etching away the AAO template completely, so that the remaining AAO template could support the thin nanotubes. The above approaches are also feasible on a glass substrate. This part deserves more study.

Compared with the ZnO films and nanorods, the ZnO nanotubes possess a better PL performance. Figure 8a shows the PL spectrum for a 180 nm thick ZnO film, nanorod, and nanotube arrays. The ZnO film and nanorods were prepared under the same deposition condition of 550 cycles at 250°C, whereas the ZnO nanotubes were
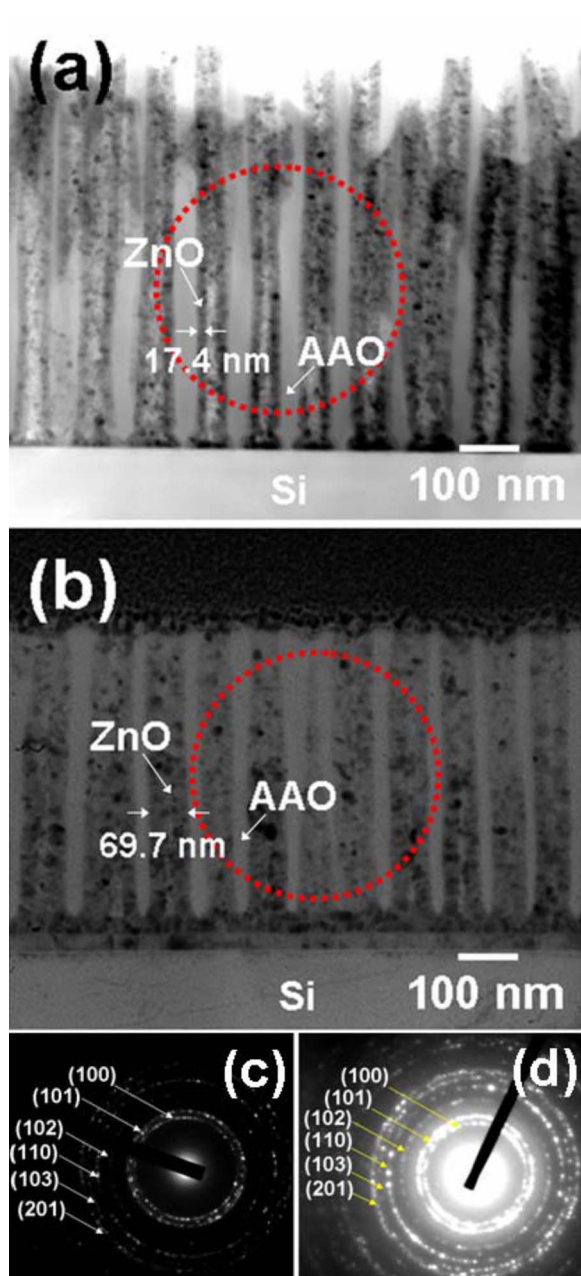
Figure 7. (Color online) Cross-sectional TEM images for (a) ZnO nanotubes with 250 cycles and (b) ZnO nanorods with 550 cycles. Figures (c) and (d) are selected area diffraction patterns for (a) and (b), respectively.

fabricated at 250 deposition cycles. For the three structures, a strong excitation emission and broad defect-level emission are observed in the UV and visible regions. After Gauss fitting, the PL spectrum can be fitted to three sub-bands (sub-band 1, sub-band 2, and sub-band 3), as shown in Fig. 8b-d. The sub-band 1 was located at 376, 379, and 377 nm, the sub-band 2 was situated at 404, 394, and 392 nm, and the sub-band 3 was observed at 612, 534, and 479 nm for the ZnO film, nanorods, and nanotubes, respectively. The sub-band 1 located at ∼380 nm is attributed to the radiation recombination of free exciton transition from the conduction band to the valance band.[39,40] The sub-bands 2 and 3 located at ∼400 to 700 nm may be caused by the defect-level transition of the oxygen vacancies and zinc interstitials, common impurities, and defects in the crystal.[39-46]

A strong excitation emission of PL (sub-band 1) is observed for the ZnO nanotubes. Shen et al. reported that both photon-to-electron conversion efficiency and photonic performance were enhanced in
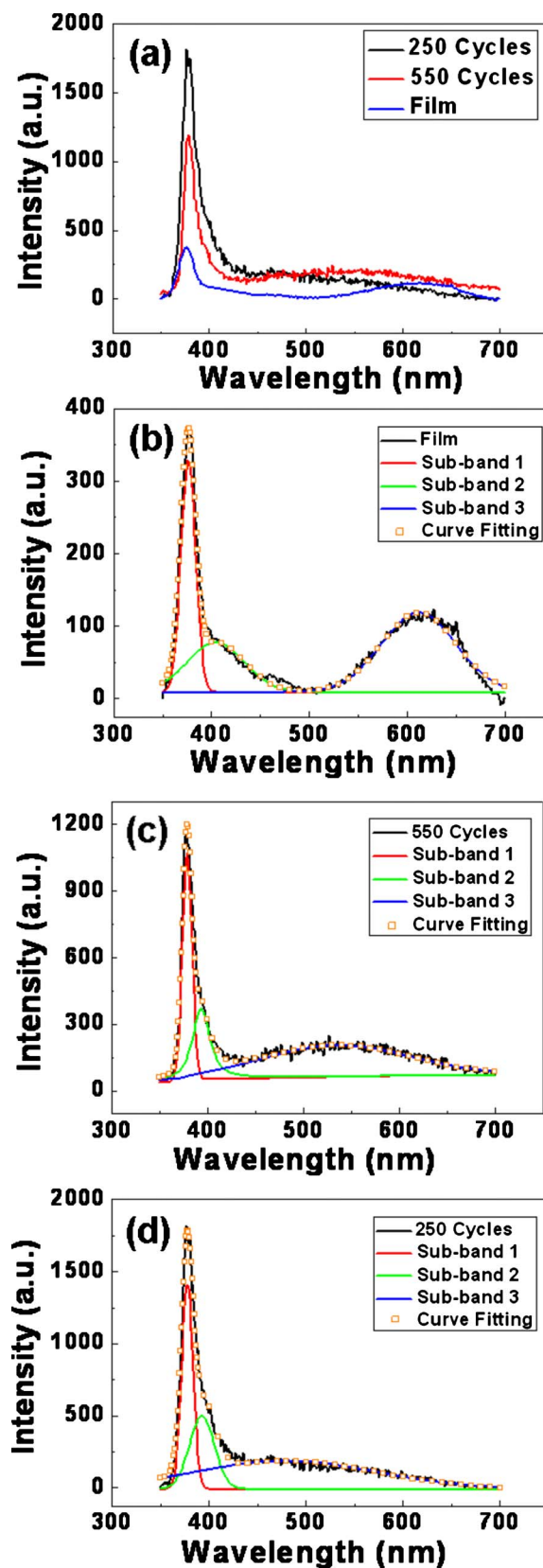

Figure 8. (Color online) (a) PL spectrum of the ZnO thin film (550 cycles), ZnO nanorods (550 cycles), and ZnO nanotubes (250 cycles). Gauss fitting was used to fit the three spectrums in (a). (b) Thin film with 550 cycles, (c) nanorods with 550 cycles, and (d) nanotubes with 250 cycles.

the studies of ZnO nanorod arrays on PL spectrum due to the decrease in diameters and the increase in surface areas for nanorod configuration.[45] In addition, Wu et al. investigated the PL spectra of ZnO nanorods and nanotubes,[40] and they found that the tubular structure is advantageous to the optical characteristic because of the higher porosity and larger surface area. In particular, for ZnO nanorods and nanotubes in this study, the surface area ratio of the nanotube to the nanorod is 1:57, which appears to fairly agree with the 1:63 ratio obtained from their area of sub-band 1 in Fig. 8c and d. Consequently, the higher excitation emission of the nanotubes could be attributed to their larger surface area. Therefore, the ZnO nanotubes exhibited better performance in excitation emission than those of the ZnO film and nanorods. In addition, a blueshift of visible emission (sub-band 3) located at $\sim$479 to 612 nm was obtained from the ZnO nanotubes, compared with the ZnO film and nanorods, in the PL spectrum. According to the literatures,[39-46] the visible band located at 479–612 nm results from the deep-level emission caused by oxygen vacancies, including $V_O^\bullet$ and $V_O^{\bullet\bullet}$. $V_O^\bullet$ is the oxygen vacancy with one electron lost at $\sim$2.0 eV below the conduction band, whereas $V_O^{\bullet\bullet}$ is the oxygen vacancy with two electrons lost at $\sim$2.2 eV below the conduction band.[39,43] Because the depletion region at the ZnO surface contains $V_O^{\bullet\bullet}$ rather than $V_O^\bullet$, this implies that the ZnO nanotubes have a larger surface area and therefore would have a large amount of $V_O^{\bullet\bullet}$. On the contrary, the ZnO film would have a higher concentration of $V_O^\bullet$ instead of $V_O^{\bullet\bullet}$. Therefore, the PL results of sub-band 3 indicate that the ZnO nanotubes would prefer to perform blue/green luminescence, whereas the ZnO film would radiate green/yellow lights. In addition, the ratio of visible emission (sub-band 3) to excitation emission (sub-band 1) is 1:73, 2:13, and 2:16 for the ZnO film, nanorods, and nanotubes, respectively. These results suggest that the ZnO nanotubes have a great amount of deep-level vacancies due to their larger surface area, which agrees well with those mentioned above. The sub-band 2 located at $\sim$400 nm may be a result of the radiation of zinc interstitials.[39,43] Nevertheless, further studies are required to clarify these results.

Conclusions

In summary, self-aligned ZnO nanotubes and nanorods have been fabricated by using ALD technique and AAO templates on Si substrates. The as-prepared AAO nanopores have a 70 nm diameter, a 95 nm pore distance, a 720 nm height, and an aspect ratio of 10:2. From the SEM and TEM images, the wall thickness of the nanotubes at 250 cycles is $\sim$18 nm and the diameter of the nanorods at 550 cycles is $\sim$70 nm. In particular, by controlling the amount of deposition cycles, the wall thickness of the nanotubes can be controlled precisely. Because of their larger surface area, the ZnO nanotubes exhibit excellent PL performances compared with the ZnO films and nanorods on the excitation emission, the blueshift of visible emission, and the ratio of visible emission to excitation emission.

Acknowledgments

References

1. Y. Xia, P. Yang, Y. Sun, Y. Wu, B. Mayers, B. Gates, Y. Yin, F. Kim, and H. Yan, *Adv. Mater.*, **15**, 353 (2003).
2. M. H. Huang, Y. Wu, H. Feick, N. Tran, E. Weber, and P. Yang, *Adv. Mater.*, **13**, 113 (2001).
3. Z. W. Pan, Z. R. Dai, and Z. L. Wang, *Science*, **291**, 1947 (2001).
4. Z. L. Wang, *J. Mater. Chem.*, **15**, 1021 (2005).
5. B. P. Zhang, N. T. Binh, K. Wakatsuki, Y. Segawa, Y. Yamada, N. Usami, M. Kawasaki, and H. Koinuma, *Appl. Phys. Lett.*, **84**, 4098 (2004).
6. Z. Y. Yuan and B. L. Su, *Colloids Surf., A*, **241**, 173 (2004).
7. Y. Lei, L. D. Zhang, G. W. Meng, G. H. Li, X. Y. Zhang, C. H. Liang, W. Chen, and S. X. Wang, *Appl. Phys. Lett.*, **78**, 1125 (2001).
8. Y. Wu, R. Fan, and P. Yang, *Nano Lett.*, **2**, 83 (2002).
9. J. Goldberger, R. R. He, Y. F. Zhang, S. Lee, H. Q. Yan, H. J. Choi, and P. Yang, *Nature (London)*, **422**, 599 (2003).
10. Z. Tang, N. A. Kotov, and M. Giersig, *Science*, **297**, 237 (2002).
11. Y. K. Tseng, C. J. Huang, H. M. Cheng, I. N. Lin, K. S. Liu, and I. C. Chen, *Adv. Funct. Mater.*, **13**, 811 (2003).
12. M. S. Arnold, P. Avouris, Z. W. Pan, and Z. L. Wang, *J. Phys. Chem. B*, **107**, 659 (2003).
13. M. Law, L. E. Greene, J. C. Johnson, R. Saykally, and P. D. Yang, *Nature Mater.*, **4**, 455 (2005).
14. S. Liang, H. Sheng, Y. Liu, Z. Huo, Y. Lu, and H. Shen, *J. Cryst. Growth*, **225**, 110 (2001).
15. Q. Wan, Q. H. Li, Y. J. Chen, T. H. Wang, X. L. He, J. P. Li, and C. L. Lin, *Appl. Phys. Lett.*, **84**, 3654 (2004).
16. S. Pizzini, N. Buttd, D. Narducci, and M. Palladino, *J. Electrochem. Soc.*, **136**, 1945 (1989).
17. N. Golego, S. A. Studenikin, and M. Cocivera, *J. Electrochem. Soc.*, **147**, 1592 (2000).
18. S. C. Minne, S. R. Manalis, and C. F. Quates, *Appl. Phys. Lett.*, **67**, 3918 (1995).
19. C. R. Gorla, N. W. Emanetoglu, S. Liang, W. E. Mayo, Y. Lu, M. Wraback, and H. Shen, *J. Appl. Phys.*, **85**, 2595 (1999).
20. M. H. Huang, S. Mao, H. Feick, H. Yan, Y. Wu, H. Kind, E. Weber, R. Russo, and P. Yang, *Science*, **292**, 1897 (2001).
21. B. Lin, Z. Fu, Y. Jia, and G. Liao, *J. Electrochem. Soc.*, **148**, G110 (2001).
22. Y. B. Li, Y. Bando, T. Sato, and K. Kurashima, *Appl. Phys. Lett.*, **81**, 144 (2002).
23. V. Craciun, R. K. Singh, J. Perriere, J. Spear, and D. Craciun, *J. Electrochem. Soc.*, **147**, 1077 (2000).
24. J. J. Robbins, J. Esteban, C. Fry, and C. A. Wolden, *J. Electrochem. Soc.*, **150**, C693 (2003).
25. J. F. Conley, Jr., L. Stecker, and Y. Ono, *Nanotechnology*, **16**, 292 (2005).
26. M. J. Zheng, L. D. Zhang, G. H. Li, and W. Z. Shen, *Chem. Phys. Lett.*, **363**, 123 (2002).
27. T. L. Sounart, J. Liu, J. A. Voigt, J. W. P. Hsu, E. D. Spoerke, Z. Tian, and Y. Jian, *Adv. Funct. Mater.*, **16**, 335 (2006).
28. H. Chik, J. Liang, S. G. Cloutier, N. Kouklin, and J. M. Xu, *Appl. Phys. Lett.*, **84**, 3376 (2004).
29. M. Scharrer, X. Wu, A. Yamilov, H. Cao, and R. P. H. Chang, *Appl. Phys. Lett.*, **86**, 151113 (2005).
30. W. H. Kim, S. J. Park, J. Y. Son, and H. Kim, *Nanotechnology*, **19**, 045302 (2008).
31. J. W. Elam, D. Routkevitch, P. P. Mardilovich, and S. M. George, *Chem. Mater.*, **15**, 3507 (2003).
32. G. Xiong, J. W. Elam, H. Feng, C. Y. Han, H. H. Wang, L. E. Iton, L. A. Curtiss, M. J. Pellin, M. Kung, H. Kung, et al., *J. Phys. Chem. B*, **109**, 14059 (2005).
33. M. S. Sander, M. J. Côté, W. Gu, B. M. Kile, and C. P. Tripp, *Adv. Mater.*, **16**, 2052 (2004).
34. D. Losic, G. Triani, P. Evans, A. Atanacio, J. Mitcheli, and N. H. Voelcker, *J. Mater. Chem.*, **16**, 4029 (2006).
35. C. J. Yang, S. M. Wang, S. W. Liang, Y. H. Chang, C. Chen, and J. M. Shieh, *Appl. Phys. Lett.*, **90**, 033104 (2007).
36. T. M. Abdel-Fattah, D. Gu, H. Baumgart, and G. Namkoong, *ECS Trans.*, **25**(4), 315 (2009).
37. F. Li, L. Zhang, and R. M. Metzger, *Chem. Mater.*, **10**, 2470 (1998).
38. O. Jessensky, F. Müller, and U. Gösele, *Appl. Phys. Lett.*, **72**, 1173 (1998).
39. Y. Y. Peng, T. E. Hsieh, and C. H. Hsu, *Nanotechnology*, **17**, 174 (2006).
40. C. C. Wu, D. S. Wuu, P. R. Lin, T. N. Chen, and R. H. Horng, *Cryst. Growth Des.*, **9**, 4555 (2009).
41. K. Vanheusden, W. L. Warren, C. H. Seager, D. R. Tallant, J. A. Voigt, and B. E. Gnade, *J. Appl. Phys.*, **79**, 7983 (1996).
42. A. van Dijken, E. A. Meulenkamp, D. Vanmaekelbergh, and A. Meijerink, *J. Lumin.*, **90**, 123 (2000).
43. S. A. M. Lima, F. A. Sigoli, M. Jafelicci, Jr., and M. R. Davolos, *Int. J. Inorg. Mater.*, **3**, 749 (2001).
44. X. L. Wu, G. G. Siu, C. L. Fu, and H. C. Ong, *Appl. Phys. Lett.*, **78**, 2285 (2001).
45. X. P. Shen, A. H. Yuan, Y. M. Hu, Y. Jiang, Z. Xu, and Z. Hu, *Nanotechnology*, **16**, 2039 (2005).
46. M. Q. Israr, J. R. Sadaf, L. L. Yang, O. Nur, M. Willander, J. Palisaitis, and P. O. Å. Persson, *Appl. Phys. Lett.*, **95**, 073114 (2009).